applied sciences

MDPI

Article

First-Principles Investigation on Type-II Aluminum-Substituted Ternary and Quaternary Clathrate Semiconductors $R_8Al_8Si_{128}$ (R = Cs, Rb), $Cs_8Na_{16}Al_{24}Si_{112}$

Dong Xue * and Charles W. Myles

Department of Physics and Astronomy, Texas Tech University, Lubbock, TX 79409-1051, USA; charley.myles@gmail.com

* Correspondence: dong.xue@ttu.edu; Tel.: +1-806-834-4563

Received: 29 November 2018; Accepted: 21 December 2018; Published: 1 January 2019

Abstract: Structural and vibrational properties of the aluminium-substituted ternary and quaternary clathrates $R_8Al_8Si_{128}$ (R = Cs, Rb), $Cs_8Na_{16}Al_{24}Si_{112}$ are investigated. The equilibrium volume of R_8Si_{136} expands when all Si atoms at the 8*a* crystallographic sites are replaced by Al. Formation of the Al–Si bond is thus anticipated to correlate with decreased guest vibration modes. Underestimation of the predicted lattice phonon conductivity κ_L (1.15 W m^{-1} K^{-1}) compared to a previous experiment (1.9 W m^{-1} K^{-1}) in $Cs_8Na_{16}Si_{136}$ is thought to arise from our evaluation on the phonon mean free path λ using the "scattering centers" model. Accordingly, we expect that the "three-phonon" processes dominate the determination of the phonon relaxation time, leading to a more reasonable λ in the $R_8Al_8Si_{128}$ system. Additionally, the "avoided-crossing" effect causes no appreciable difference in the sound speed for acoustic phonons in this framework. Starting with configuration optimization about aluminium arrangements in $Cs_8Na_{16}Al_{24}Si_{112}$, the calculated lattice parameter agrees well quantitatively with the experiment. The reduced U_{iso} of Cs from this calculation is anticipated to be primarily related to temperature-dependent quartic anharmonicity. Meanwhile, the predicted κ_L for $Cs_8Na_{16}Al_{24}Si_{112}$ remains not sensitive to the Al arrangement on 96*g* Wyckoff sites.

Keywords: ternary clathrate; quaternary; anharmonicity; avoided-crossing; scattering centers

1. Introduction

Ternary and quaternary clathrate compounds have been the subject of growing interest in recent years [1–6]. Here, the terms "ternary" and "quaternary" refer to a chemical substance that contains three and four distinct elements, respectively. Generally, clathrate compounds are classified as one of two categories: Type-I and Type-II. The unit cell of a Type-I compound configuration possesses a simple cubic framework that accommodates a limited integer number of guest atoms placed inside the polyhedron structure, which is a 20-atom or 24-atom cage. Similarly, the framework of a Type-II compound is made of 20- and 28-atom cages connected in a ratio of 2:1, leading to encapsulation of the guest atoms. Moreover, the clathrate framework serving as the host can be formulated by one Group-IV element (Si, Ge, Sn) or a mixture of any single type of Group-IV element and another type of Group-III atoms (usually Al or Ga). Specifically, the usage of Al or Ga atoms is selected to compensate for excess valence electrons arising from guest atoms in order to make the entire compound semiconducting. That is, the Zintl phase criteria [7] is satisfied after such Group-III atoms are substituted onto the framework site in the presence of alkali or alkali earth guests. Another unique characteristic of the clathrate compound structure is the flexibility of filling two different guest atom types rather than a single type into two different sized cages. Previously, ternary and quaternary clathrate compounds,

including $Sr_8Ga_xSi_{46-x}$, $X_8Ga_{16}Ge_{30}$ (X = Eu, Sr, Ba), $Ba_8Zn_xGe_{46-x-y}Si_y$, and $(Ba,Sr)_8Ga_{16}Si_xGe_{30-x}$, have been undergoing intensive study [8–13].

In contrast to investigations on pure clathrate, such as open framework Si_{46}, Ge_{46}, Si_{136}, or intermetallic binary clathrate systems Ba_xSi_{46}, A_xSi_{136} (A = alkaline metal; $0 < x \leq 24$) [14–18], little is understood about Type-II ternary and quaternary clathrate compounds as opposed to Type-I counterparts. Therefore, in this work we decided to intensively study Si-based Type-II materials $R_8Al_8Si_{128}$ (R = Cs, Rb) and $Cs_8Na_{16}Al_{24}Si_{112}$. These materials are of great importance due to their unique thermodynamical properties. Specifically, the existence of low-energy, localized optic modes arising from guest "rattlers" cause the acoustic phonon spectrum to exhibit an "avoided-crossing" effect. Therefore, the suppression of acoustic phonon bands might have an inherent interaction with increased anharmonicity in these semiconducting systems. Consequently, a reevaluation of the phonon lifetime is needed because the three-phonon process begins to dominate over other scattering models derived from a harmonic approximation point of view. In this paper, significant details will also be discussed on the underestimation of the lattice thermal conductivity when considering the neighboring distance of guest rattlers as the phonon mean free path. In other words, the primitive model, which suggests that guest atoms act as scattering centers, needs to be readjusted because of the large phonon thermal conductivity observed in $Cs_8Na_{16}Si_{136}$.

In addition, we studied the impact of different substitutional framework atoms on the thermodynamic natures of these semiconducting clathrates (e.g., $Cs_8Ga_8Si_{128}$ and $Cs_8Al_8Si_{128}$) of interest. We found an acoustic band difference exists for lattice vibration when comparing the compound $R_8Al_8Si_{128}$ (R = Cs, Rb) to its "parent" Al_8Si_{128} framework. Moreover, we examined how the formation of Al–Si bonds affects the structural properties of $R_8Al_8Si_{128}$ after all Si atoms at the 8*a* Wyckoff sites are completely replaced by Al. To simulate clearly the site occupancies of Al on the three crystallographic sites for the parent "$Al_{24}Si_{112}$" suggested by the experimental work, we test a limited number of configurations and determine the most energetically favorable geometry for $Cs_8Na_{16}Al_{24}Si_{112}$. Using the best refined configuration along with other possible types, we present our predictions for the lattice constant (a), bulk modulus (K), temperature-dependent atomic displacement parameters (U_{iso}) and lattice thermal conductivity (κ_L).

2. Computational Approach

Our first-principles calculations are based on the local density approximation (LDA) to the density functional theory and have utilized the Vienna ab initio Simulation Package (VASP) [19]. Here, the self-consistent Kohn–Sham equations [20] are solved in the LDA calculations. To approximate the exchange-correlation energy term, we used the Ceperly–Alder functional. This technique has been used in previous investigations of Si and Ge clathrates [16,21–23]. Starting with structural optimization, we determine the lattice constant at the equilibrium geometry through a conjugate gradient (CG) algorithm. The energy cutoff parameter here is selected to be a default value (245.7 eV) according to pseudopotentials obtained from the projector augmented wave (PAW) method. Next, several pairs of acquired data describing the LDA energy vs. volume are fitted to the third-order Birch–Murnaghan equation of state (EOS) [24], giving rise to an energy–volume relation. Such a fitting procedure yields a determination on the equilibrium energy E_0, equilibrium volume V_0, bulk modulus K and K's pressure derivative $K' = dK/dP$ at absolute zero temperature. It is also noted that the total energy convergence is adjusted to be 10^{-7} eV.

The vibrational properties are calculated using the harmonic approximation in VASP. Our approach to conduct the predicted phonon dispersion curves, along with the subsequently derived effective force constant for the guest "rattlers" in the Si hexakaidecahedron cage, is summarized as follows. The first step is to obtain the dynamical matrix $\boldsymbol{D}(\boldsymbol{q})$ after moving each guest atom initially located at the Si_{28} cage center by a small finite displacement ($U_0 = 0.02$ Å), in the presence of a $2 \times 2 \times 2$ $\boldsymbol{k}$-point grid [25] as well as for wave vectors in the vicinity of the gamma (Γ) point [$\boldsymbol{q}$ = (0,0,0)]. Second, diagonalization of the dynamical matrix $\boldsymbol{D}(\boldsymbol{q})$ allows us to determine the vibrational eigenvalues

$\omega^2(\boldsymbol{q})$ (squared frequencies) and eigenvectors. On the basis of derived acoustic phonon spectrum arising from the knowledge of $\boldsymbol{D}(\boldsymbol{q})$, we predict the lattice thermal conductivity through simple kinetic theory, $\kappa_L = (1/3)C_v v_s \lambda$ [26], where the mean free path λ is evaluated as the separation distance between the neighboring guests encapsulated in adjacent hexakaidacahedron cage. Furthermore, the inverse cubic of phonon velocity of sound v_s is obtained through the average of the inverse third power of the long-wavelength phase velocities of the three acoustic modes (see subscript i): $1/(v_s)^3 = 1/3\sum\int(1/(\mathrm{d}\omega_i(\boldsymbol{q})/\mathrm{d}\boldsymbol{q})^3)(1/4\pi)\mathrm{d}\Omega$. C_v is the specific heat per unit volume. Other property such as atomic displacement parameters can be gained from the localized, flat vibrational modes of guest rattling.

3. Results

3.1. Ternary Clathrate $Cs_8Al_8Si_{128}$ and $Rb_8Al_8Si_{128}$

The LDA-calculated lattice constant, bulk modulus and cohesive energy per atom in the presence of Al-substituted and Ga-substituted binary, ternary compounds are listed in Table 1. Here, Ga appearing in $(Cs,Rb)_8Ga_8Si_{128}$ has an s^2p^1 valence electronic configuration, making it possible for it to behave as an electron acceptor while compensating for excess valence electrons that arise from guest impurity according to the Zintle–Klemm criteria [7]. It is noted that all Al atoms subjected to their occupied 8*a* Wyckoff sites can form an Al-Si bond in the case of $(Rb,Cs)_8Al_8Si_{128}$. Intriguingly, our density functional theory (DFT) work shows the entire lattice structure experiences a slight expansion when all Si atoms at the 8*a* Wyckoff sites are completely replaced by Al. From the viewpoint of fundamental chemistry, aluminum is classified as a Group-III element, which has a reduced atomic mass (approximately 4% lighter than Si) and a smaller radius. In contrast, the lattice constant of $Cs_8Al_8Si_{128}$ (14.676 Å) is computed to remain approximately 0.64% larger than that of Cs_8Si_{136} (14.583 Å). This discrepancy in terms of the structural change allows one to anticipate the correlation between the framework bonding formation Al–Si and guest–host coupling. Our results give rise to approximately 41.1 cm^{-1} for Cs vibration frequency ω in $Cs_8Al_8Si_{128}$ (see Figure 1), which is approximately 5.9% lower than that of Cs_8Si_{136}. The suppressed Cs vibration frequency in the Al-substituted compound $Cs_8Al_8Si_{128}$ is an indicative of its relatively weakly bound behavior with respect to cage constituents. In other words, the Cs guest has slightly more room to move around inside the cage, resulting in an occurrence of geometry dilation.

Table 1. The equation of state (EOS) parameters obtained for the filled ternary clathrate $(Rb,Cs)_8Al_8Si_{128}$, $(Rb,Cs)_8Ga_8Si_{128}$ and binary clathrate $(Cs,Rb)_8Si_{136}$.

Material	*a* (Å)	E_0 (eV/atom)	*K* (Gpa)	d*K*/d*P*
$Rb_8Al_8Si_{128}$	14.669	−5.555	78.428	4.172
$Cs_8Al_8Si_{128}$	14.676	−5.573	80.385	3.082
$Rb_8Ga_8Si_{128}$	14.644	−5.536	79.063	5.054
$Cs_8Ga_8Si_{128}$	14.651	−5.555	79.735	4.085
Cs_8Si_{136}	14.583	−5.694	82.783	5.205
Rb_8Si_{136}	14.572	−5.681	83.115	4.955

Our results in Table 1, which describe the structural property of Rb-containing ternary compounds, yield a similar lattice constant: 14.670 Å for $Rb_8Al_8Si_{128}$ and 14.644 Å for $Rb_8Ga_8Si_{128}$. Analogous to the expanded volume found in $Cs_8Al_8Si_{128}$ compared with Cs_8Si_{136}, lattice framework expansion also occurs in $Rb_8Al_8Si_{128}$ when all Si atoms at the 8*a* Wyckoff sites are replaced by Al atoms in Rb_8Si_{136}. The rattling modes of Rb in $Rb_8Al_8Si_{128}$ show frequencies of 31.3 cm^{-1}, which are approximately 17.4% smaller than the value of the guest vibration in Rb_8Si_{136}. Therefore, it is further expected that the formation of the Al–Si bond other than the Si–Si bond might participate in minimizing the effective force constant of the Rb rattler, leading to a suppressed Rb vibration.

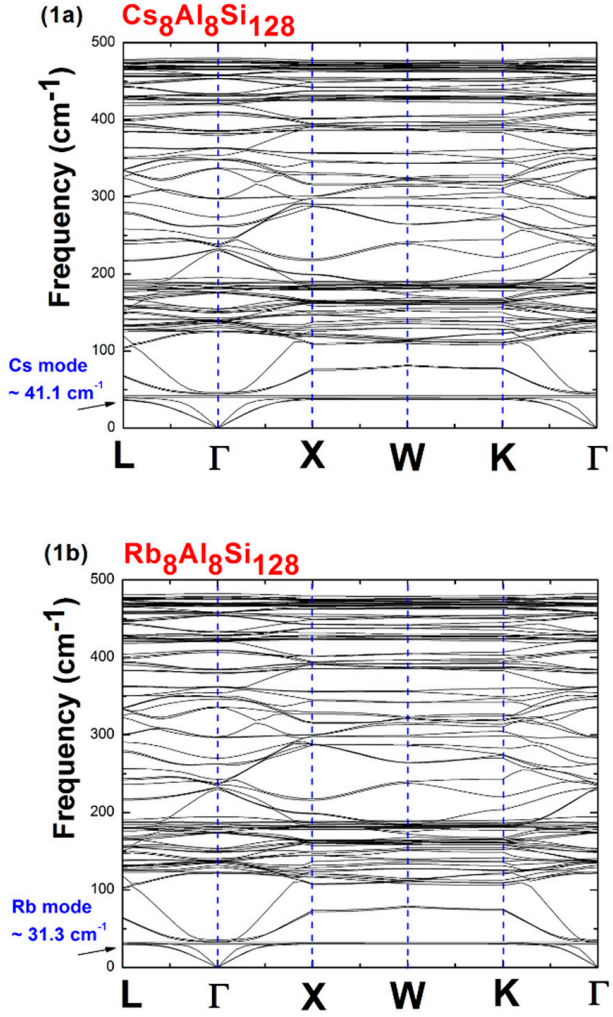

Figure 1. Phonon dispersion relations of: (**a**) $Cs_8Al_8Si_{128}$ and (**b**) $Rb_8Al_8Si_{128}$.

Using a harmonic oscillator model [27], $\omega = (\varphi/M)^{1/2}$, where M represents the mass of the guest, the estimated effective force constant φ of Cs is 0.85 eV Å^{-1} in $Cs_8Al_8Si_{128}$ and 0.96 eV Å^{-1} in Cs_8Si_{128}. The values of φ for Rb modes in $Rb_8Al_8Si_{128}$ (see Figure 1) and Rb_8Si_{128} are calculated to be 0.31 and 0.46 eV Å^{-1}, respectively. Furthermore, an estimation on the Al–Si bond length and Si–Si bond length are based on the nearest neighboring distance table from our LDA calculation. The average Al–Si bond length is computed to be 2.42 Å, while the average Si–Si bond length is 2.32 Å. This difference has been identified to be relevant with a structural change upon the partial framework substitution.

The physical origin of the lattice structure response upon the framework substitution might be connected to the altered guest–host interaction strength due to the Al–Si formation. In Figure 1, one of the notable features for low-frequency (<200 cm^{-1}) vibration spectrum is the nondispersive and flat optic modes, whose frequencies remain at nearly 41.1 cm^{-1} and 31.3 cm^{-1} for $Cs_8Al_8Si_{128}$ and $Rb_8Al_8Si_{128}$, respectively. Accordingly, the determined vibrational density of states (VDOS) denoted by $g(\omega)$ is shown in Figure 2, displaying the acoustic phonon bandwidth (<115 cm^{-1}) along with the rattling optical modes (Cs, Rb mode). $g(\omega)$ is normalized such that $\int g(\omega)\, d\omega = 3N$, where N is the total number of atoms in the primitive unit cell when the frequency ω is limited to the entire phonon region (<500 cm^{-1}). The Debye approximation which assumes that acoustic phonon branches have linear dispersion relation within first Brillouin zone is taken into account to calculate phonon density of states in Figure 2. Meanwhile, the projected density of states is obtained by summation of that contribution over flat, localized optical phonon bands due to guest rattler (Cs, Rb) in the same diagram.

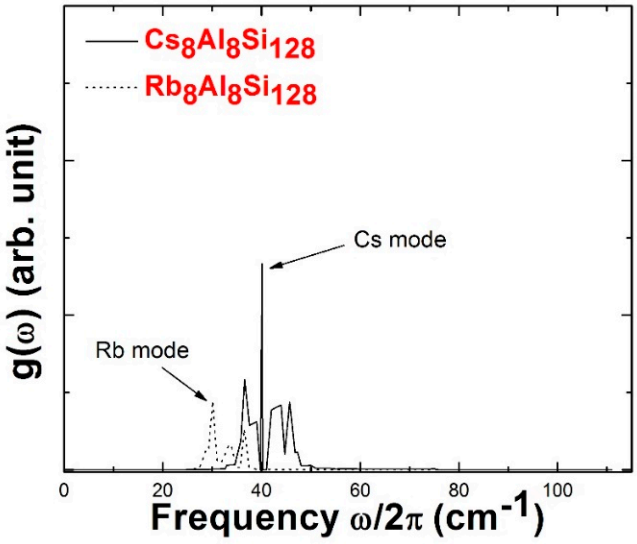

Figure 2. Calculated vibrational density of states (VDOS) vs. frequency for $Cs_8Al_8Si_{128}$ (solid line) and $Rb_8Al_8Si_{128}$(dotted line).

On the other hand, the group velocity for the lowest-lying acoustic phonons in these ternary compounds are almost independent of the guest type, remaining unaffected when compared with Al_8Si_{128} in Figure 3.

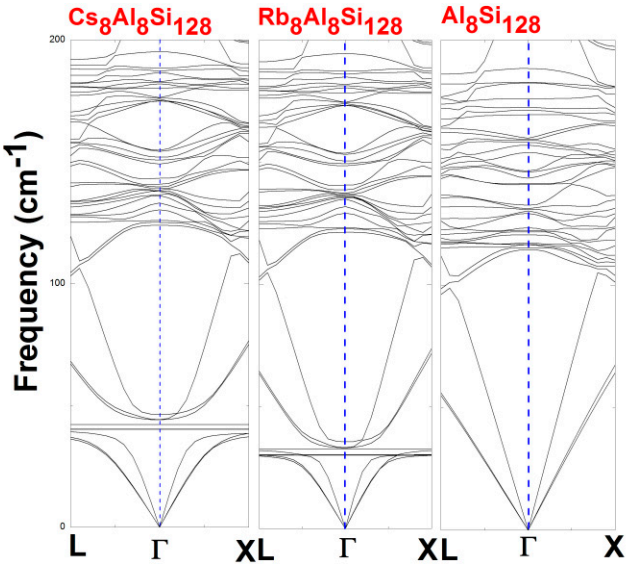

Figure 3. Predicted low-frequency vibration spectrum of $Cs_8Al_8Si_{128}$,$Rb_8Al_8Si_{128}$ and Al_8Si_{128}.

Numerical calculation involving diagonalization of the dynamical matrix verifies that these localized optic bands are essentially due to the guest motion. Comparing these low-lying optic modes to that of the dispersion relation of Al_8Si_{128} in Figure 3, one sees the "bending" of the acoustic branches, in which the frequency is supposed to extend to approximately 120 cm^{-1}. This is indicative of a strong coupling between the localized Cs (or Rb) modes and acoustic phonon bands, which carry thermal energy. Therefore, these resonant couplings are identified as "avoided-crossing effect", allowing phonon branches of the Cs (or Rb) and Al_8Si_{128} framework to meet and avoid one another near 41 cm^{-1} and 31 cm^{-1} in the $Cs_8Al_8Si_{128}$ and $Rb_8Al_8Si_{128}$ material, respectively.

The lattice vibration contribution to the thermal conductivity in some semiconducting clathrate compounds were found to play a dominant role in comparison with the relatively small electronic

contribution [28–30]. An evaluation on the electronic thermal conductivity can be facilitated by combining the resistivity ρ measurements and the Wiedemann-Franz relation ($\kappa_e = L_0 T\rho$, where L_0 = 2.45 × 10^{-8} W Ω K^{-2}) [31]. A negligible κ_e is normally characterized by a quite large resistivity whose value remains beyond the scope of 10 mΩ·cm [28,29]. Due to similar reasons, the lattice thermal conductivity of ternary clathrate $(Cs,Rb)_8Al_8Si_{128}$ is given essential importance here. Inspired by the previously suggested "rattling" model [32], which states guest impurity resonantly vibrates with the cage constituent, one becomes familiar with the minimization of lattice thermal conductivity. This suppression is furnished when the glass-like phonons, which carry thermal energy, are scattered by a large scale of loosely bound "rattlers". Accordingly, our estimated lattice vibration contribution to the thermal conductivity are given from a simple kinetic equation $\kappa_L = (1/3)C_V v_s \lambda$. Here, λ is also assumed that such neighboring guests act as almost localized "scattering centers". Consequently, we predict the lattice thermal conductivity (see Table 2) of the ternary compound $Cs_8Na_{16}Si_{136}$, whose value remains lower than the experimental data [23]. To account for this increased κ_L arising from the observed measurement, we anticipate that the lattice thermal conductibility is strongly affected by the avoided-crossing effect caused by flat localized phonons rather than guest atoms that serve as scattering centers. In other words, the mean free path of acoustic phonons (transverse acoustic (TA) and longitudinal acoustic (LA)) near the avoided-crossing point might be recalculated due to the predominant three-phonon processes suggested by Ref. [33,34]. The previously used separation of rattlers (Cs–Cs distance ~ 6.34 Å) shows an underestimation on the mean free path. It is noted that the relation $\lambda_q = v_q \tau_q$ helps to find the mean free path λ_q of acoustic phonons in the presence of a computed phonon lifetime τ_q while considering cubic anharmonicity originating from three-phonon interaction [34]. Specifically, the phonon lifetime τ_q due to anharmonic phonon scattering is determined by the inverse of imaginary part of bubble self-energy, which remains roughly proportional to summation corresponding to the strength of the cubic coupling. Previously, the computation of κ_L based on the phonon lifetime of the TA, LA mode due to the "avoided-crossing" effect leads to a quantitatively good agreement with the experimental data [34–37].

Table 2. Local density approximation (LDA)-performed rattling mode ω, group velocity of transverse acoustic (TA) phonons v_{TA}, group velocity of longitudinal acoustic (LA) phonons v_{LA}, sound velocity v_s, phonon mean free path λ and lattice thermal conductivity κ_L for filled ternary clathrate $(Rb,Cs)_8Al_8Si_{128}$, $Cs_8Na_{16}Si_{136}$ and $(Cs,Rb)_8Si_{136}$.

Material	ω (cm^{-1})	v_{TA} (ms^{-1})	v_{LA} (ms^{-1})	v_s (ms^{-1})	λ (Å)	κ_L ($Wm^{-1}K^{-1}$)
$Rb_8Al_8Si_{128}$	31.1	3010	5179	3161	6.35	1.05
$Cs_8Al_8Si_{128}$	41.1	2744	5134	3065	6.35	1.01
$Cs_8Na_{16}Si_{136}$	45.5	2728	4895	3038	6.34	1.15(1.9 *)
Cs_8Si_{136}	43.7	2983	5373	3322	6.31	1.10
Rb_8Si_{136}	37.9	3028	5496	3375	6.31	1.12

* Reference [32].

Figure 4 shows the "avoided-crossing" effect because of guest-host coupling with respect to $Cs_8Al_8Si_{128}$ along the Γ-X line. The dotted lines describing the dispersive LA and TA phonons of Al_8Si_{128} are also given for comparison. It is shown that those crossings due to the "intersection" of the flat localized Cs modes appear roughly at 40–41 cm^{-1}. Specifically, crossings of TA phonons and LA phonons occur at approximately 3/5 and 3/10 along the Γ-X line. The consequence of these "avoided-crossings" is attributable to strong interactions between the acoustic phonons and rattling modes. Near the crossing point, which is below the optic band of Cs, the group velocity of TA and LA phonons is facing substantial reduction ($v_{TA(LA)} \rightarrow 0$). This indicates that the phonon-rattler coupling is dominantly modeled by three-phonon processes at crossings. The suggested $\lambda_q = v_q \tau_q$ can be used to evaluate the mean free path in a more reasonable way, resulting in a good agreement with the experimentally determined κ_L.

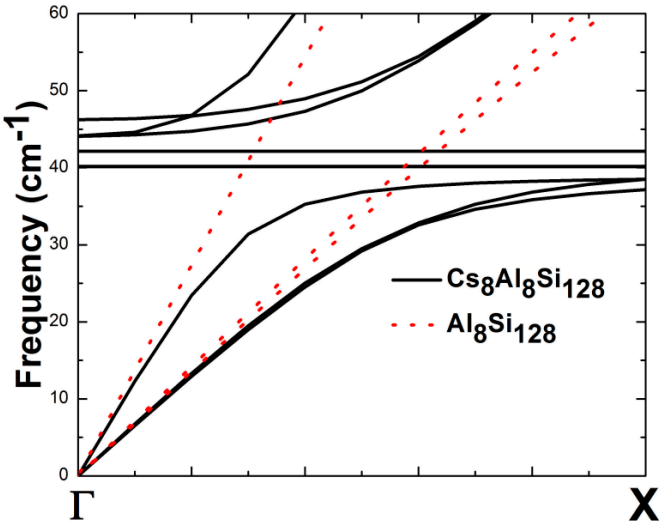

Figure 4. "Avoided-crossing" effect due to encapsulated Cs introduced into Al_8Si_{128}. The solid line shows low-frequency dispersion relation curves of $Cs_8Al_8Si_{128}$ along the Γ–X direction. Dotted lines give dispersion relation curves of Al_8Si_{128}.

Another feature regarding the guest resonant vibration is the rattler's impact on sound velocity. It is determined by our first-principles calculation (Figure 3) that little suppression of v_s concerning acoustic phonons is found by means of framework substitution upon Al, which replaces the Si atoms on the 8*a* Wyckoff sites. Meanwhile, no appreciable difference is shown with the group velocities of LA phonons as well as the sound velocity in $Cs_8Al_8Si_{128}$ and $Rb_8Al_8Si_{128}$ (see Figure 3). The above table demonstrates our predicted group velocity for different acoustic phonon modes along with the macroscopic velocity (v_s) in a detailed manner.

From Table 2, our predicted lattice thermal conductivity of $Cs_8Na_{16}Si_{136}$ yields 1.15 W m^{-1} K^{-1}, which stays lower than that of the experimental work (1.9 W m^{-1} K^{-1}). This is indicative of the fact that the phonon mean free path is underestimated. This induced underestimation might be due to an inappropriate usage of the neighboring guest–guest distance (6th column of Table 2). As discussed in some reports [34–36], the dominant "three-phonon" processes were proposed here to govern the phonon-rattling interaction due to "avoided-crossing", leading to a reasonable evaluation on the mean free path. Therefore, it seems necessary to recompute the phonon lifetime of acoustic phonons near the avoided crossing point and to obtain a more reliable estimation on κ_L.

3.2. *Quaternary Clathrate $Cs_8Na_{16}Al_{24}Si_{112}$*

Quaternary clathrate $Cs_8Na_{16}Al_{24}Si_{112}$ can be favorably formed by a kinetically controlled thermal decomposition (KCTD) approach, which was performed by K. Wei et al. [38]. Our conducted LDA work presents some structural, vibrational and thermodynamics properties of this compound for comparison. According to both Rietveld refinement and an elemental analysis, the crystallographic site details of Al and the atomic displacement parameter (ADPs) of Cs (Na) are measured in their work. The suggested refinement of the framework site occupancy shows Al/Si ratio values of 0.2/0.8 for 8*a*, 0.1/0.9 for 32*e*, and 0.2/0.8 for the 96*g* Wyckoff site. To closely simulate the occupancy of Al on these crystallographic sites using the LDA approach, we testify a limited number of possible ways (see Table 3) of arranging these substituted Group-III atoms. It is determined that the lowest energy configuration possesses a total energy of −200.68 eV per unit cell. For the most energetically stable structure of the $Al_{24}Si_{112}$ framework in our study, it has zero Al atoms on 8*a* sites, while 32*e* and 96*g* sites are partially occupied by four and 20 Al atoms in the unit cell, respectively. Taking the occupancy of Al on the 96*g* sites into account, our calculation shows the favored configuration that yields the highest Al/Si ratio value of 0.208/0.792.

Table 3. The occupancy of framework atoms (Al, Si) on different Wyckoff sites, including 8*a*, 32*e*, 96*g* and the EOS parameters for the energetically stable configuration (the second row) as well as other configurations.

8*a* (Al1/Si1)	32*e* (Al2/Si2)	96*g* (Al3/Si3)	*a* (Å)	*K* (GPa)	Δ*E* (meV)
0/1	0.125/0.875	0.208/0.792	14.9147	70.41	0
(0.2/0.8) *	(0.1/0.9) *	(0.2/0.8) *	(14.9153 *)		
0/1	0.25/0.75	0.167/0.833	14.9103	70.92	157
0.5/0.5	0.25/0.75	0.125/0.875	14.8947	71.00	520
1/0	0.5/0.5	0/1	14.8861	71.35	914

* Reference [38].

Additionally, the energy difference Δ*E* between the lowest energy and those of the remaining configurations are listed in the last column of Table 3. Our LDA calculations on seeking the most stable configuration agree fairly well with the refined data on the Al occupancy on each framework site according to the powder X-ray diffraction (PXRD) measurements. The parameters in parentheses of Table 3 were obtained from Rietveld refinement, characterizing crystal compositions of the $Cs_8Na_{16}Al_{24}Si_{112}$ host framework. Moreover, we found that a decreased number of occupied 96*g* sites by the Al element causes the total energy to increase. Accordingly, the structural contraction accompanied by a descendant lattice constant occurs with the reduced occupancy ratio of Al/Si residing on the 96*g* site. It is necessary to mention that the digit 1 appearing in notation Si1/Al1 denotes the 8*a* site, while digits 2 and 3 in Si2/Al2 and Si3/Al3 correspond to the 32*e* and 96*g* sites, respectively. Among the listed four configurations of $Cs_8Na_{16}Si_{24}Si_{112}$, it is also seen that the calculated lattice constant of the most favourable geometry (14.9147 Å) shows greater similarity to the experimental result (14.9153 Å) than other configurations.

Our predicted thermal performance, such as isotropic atomic displacement parameters U_{iso} (ADPs) and lattice thermal conductivity are illustrated in the figures below (Figures 5 and 6). The dependence on the substituted Al composition of the lattice thermal conductivity is given at $T = 300$ K. It is determined that the overestimation on U_{iso} for a quaternary compound $Cs_8Na_{16}Al_{24}Si_{112}$ occurs between the DFT-results and XRD data, making it possible to reconsider the validity of the quantized harmonic oscillator model. It is expected that the temperature-dependent quartic anharmonicity plays a dominant role in increasing the rattling frequency of the guest impurity at $T = 300$ K, leading to a reduced U_{iso} value. In other words, predicting the Cs rattling behavior from the harmonic oscillator model in $Cs_8Na_{16}Al_{24}Si_{112}$ needs to be reconsidered unless the self-consistent phonon (SCP) model [39] is applied to derive the temperature-dependent frequency of guest vibration. Moreover, the given nominal composition with respect to the Al occupancy on each framework site is anticipated to influence the U_{iso} in a slight fashion. The Cs vibration mode in $Cs_8Na_{16}Ge_{136}$ was also employed to compute the isotropic atomic displacement parameters at a specified temperature in the previous work [22], leading to a good quantitative agreement with the calculated U_{iso} regarding Cs motion in $Cs_8Na_{16}Al_{24}Si_{112}$ configurations. Such similar trends are interpreted as meaning that the "tuned" parent framework switched from "$Al_{24}Si_{112}$" to "Ge_{136}" does not effectively impact the rattling frequency.

It is notable that the predicted κ_L is not sensitive to a different Al occupancy on the host sites (96*g*) in Figure 6. The dotted line acts as a guile for the eye, showing the Al3/Si3 composition independence with respect to κ_L. This yields approximately 1 W m^{-1} K^{-1} for the predicted lattice thermal conductivity.

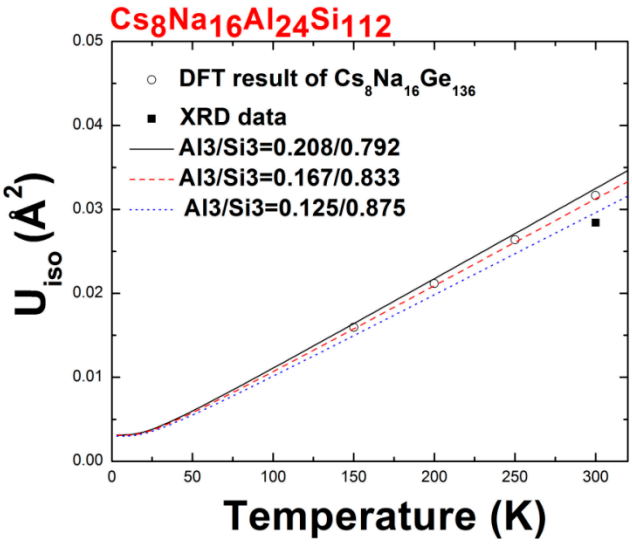

Figure 5. Theoretically and experimentally estimated isotropic atomic displacement parameters (U_{iso}) of Cs in the 28-cage. The open symbols represent the data corresponding to Cs vibration in $Cs_8Na_{16}Ge_{136}$ [22]. The solid symbol denotes the measured value of U_{iso} regarding Cs rattling in $Cs_8Na_{16}Al_{24}Si_{112}$.

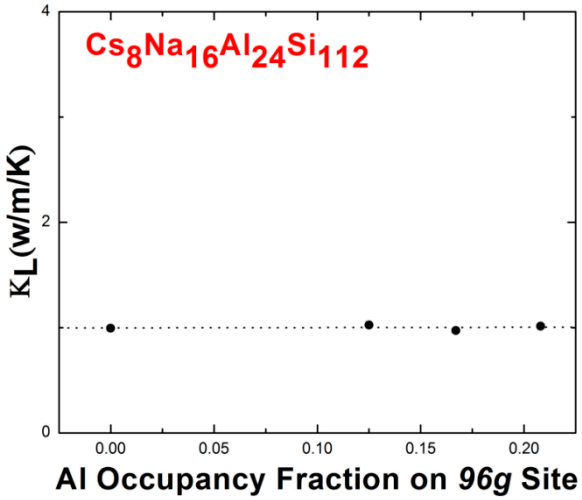

Figure 6. The predicted lattice thermal conductivity as a function of Al occupancy on the 96*g* Wyckoff site. The dotted line is used for comparison.

In contrast to the measured κ_L (~4.5 W m^{-1} K^{-1}) [38], the 4-fold reduction of lattice thermal conductivity still questions the validity of the resonant "scattering centers" model relating to acoustic phonons. Instead, the cubic anharmonicity effect needs to be reviewed in order to achieve a quantitative agreement between the first-principles calculation and experimentally observed κ_L in quaternary system $Cs_8Na_{16}Al_{24}Si_{112}$.

4. Conclusions

We report a systematic first-principles investigation on the structural and vibrational properties of $R_8Al_8Si_{128}$ (R = Cs, Rb) and $Cs_8Na_{16}Al_{24}Si_{112}$ clathrates. Among them, vibration of the rattler in Al-substituted ternary clathrate $R_8Al_8Si_{128}$ produces lower rattling modes than that of the same rattler in R_8Si_{128}. Therefore, it is anticipated that the formation of Al–Si might participate in a minimization of the guest rattling frequency in $(Cs,Rb)_8Al_8Si_{128}$, compared to that of $(Cs,Rb)_8Si_{136}$. Moreover, the validity of the resonant rattling model where the acoustic phonon can travel between

the neighboring scattering center to the exchange thermal energy is reconsidered for materials studied here, since this scheme induces underestimation on predicted lattice thermal conductivity. Instead, computing the phonon lifetime governed by three-phonon processes near the crossing in $R_8Al_8Si_{128}$ and $Cs_8Na_{16}Al_{24}Si_{112}$ is preferred. In addition to this, the "avoided-crossing" effect causes no appreciable difference when evaluating the acoustic phonon speed to exist. The optimized geometry for $Cs_8Na_{16}Al_{24}Si_{112}$ is determined theoretically when Al/Si ratio has values of 0.2/0.8 for the 8*a* Wyckoff sites, 0.1/0.9 for the 32*e* sites and 0.2/0.8 for the 96*g* sites, according to the suggested refinement from the experimental point of view. The calculated atomic displacement parameters (ADPs) of Cs for every possible composite structure of $Cs_8Na_{16}Al_{24}Si_{112}$ are larger than the XRD-determined result at T = 300 K. This overestimation is thought to be attributable to the temperature-dependent quartic anharmonicity effect of guest vibration.

Author Contributions: D.X., the first author, undertook all of the (sometimes computationally intense) calculations that are reported in the paper. He also wrote the majority of the first draft and participated in the editing of that draft which produced the final, submitted version. C.W.M., the second author, is a Professor of Physics and Astronomy at Texas Tech University. He is the PhD research advisor to D.X.

Funding: This research received no external funding.

Acknowledgments: We would like to acknowledge grateful discussions with M. Sanati (Texas Tech University) about the use of VASP. We also appreciate many hours of computing time at the High Performance Computing Center of Texas Tech University.

Conflicts of Interest: The authors declare no conflict of interest.

References

1. Melnychenko-Koblyuk, N.; Grytsiv, A.; Fornasari, L.; Kaldarar, H.; Michor, H.; Rohrbacher, F.; Koza, M.; Royanian, E.; Bauer, E.; Rogl, P. Ternary clathrates Ba-Zn-Ge: Phase equilibria, crystal chemistry and physical properties. *J. Phys. Condens. Matter* **2007**, *19*, 216223. [CrossRef]
2. Nasir, N.; Grytsiv, A.; Melnychenko-Koblyuk, N.; Rogl, P.; Bauer, E.; Lackner, R.; Royanian, E.; Giester, G.; Saccone, A. Clathrates $Ba_8\{Zn,Cd\}_xSi_{46-x}$, $x \sim 7$: Synthesis, crystal structure and thermoelectric properties. *J. Phys. Condens. Matter* **2009**, *21*, 385404. [CrossRef] [PubMed]
3. Okamoto, N.L.; Kishida, K.; Tanaka, K. Effect of in additions on the thermoelectric properties of the type-I clathrate compound $Ba_8Ga_{16}Ge_{30}$. *Appl. Phys.* **2007**, *101*, 113525. [CrossRef]
4. Takasu, Y.; Hasegawa, T.; Ogita, N.; Udagawa, M.; Avila, M.A.; Suekuni, K.; Ishii, I.; Suzuki, T.; Takabatake, T. Dynamical properties of guest ions in the type-I clathrate compounds $X_8Ga_{16}Ge_{30}$ (X= Eu, Sr, Ba) investigated by Raman scattering. *Phys. Rev. B* **2006**, *74*, 174303. [CrossRef]
5. Kishimoto, K.; Ikeda, N.; Akai, K.; Koyanagi, T. Synthesis and thermoelectric properties of silicon clathrates $Sr_8Al_xGa_{16-x}Si_{30}$ with the Type-I and Type-VIII structures. *Appl. Phys. Express* **2008**, *1*, 031201. [CrossRef]
6. Shimizu, H.; Takeuchi, Y.; Kume, T.; Sasaki, S.; Kishimoto, K.; Ikeda, N.; Koyanagi, T. Raman spectroscopy of type-I and type-VIII silicon clathrate alloys $Sr_8Al_xGa_{16-x}Si_{30}$. *J. Alloy. Compd.* **2009**, *487*, 47–51. [CrossRef]
7. Santamaria-Perez, D.; Vegas, A. The Zintl-Klemm concept applied to cations in oxides. I. The structures of ternary aluminates. *Acta Cryst. B* **2003**, *59*, 305–323. [CrossRef]
8. Imai, M.; Nishida, K.; Kimura, T.; Yamada, K. Synthesis of a Si-clathrate compound, $Sr_8Ga_xSi_{46-x}$, and its electrical resistivity measurements. *J. Alloy. Compd.* **2002**, *335*, 270–276. [CrossRef]
9. Sales, B.C.; Chakoumakos, B.C.; Jin, R.; Thompson, J.R.; Mandrus, D. Structural, magnetic, thermal, and transport properties of $X_8Ga_{16}Ge_{30}$ (X= E u, S r, Ba) single crystals. *Phys. Rev. B* **2001**, *63*, 245113. [CrossRef]
10. Nasir, N.; Grytsiv, A.; Melnychenko-Koblyuk, N.; Rogl, P.; Bednar, I.; Bauer, E. Crystal structure and physical properties of quaternary clathrates $Ba_8Zn_xGe_{46-x-y}Si_y$, $Ba_8(Zn,Cu)_xGe_{46-x}$ and $Ba_8(Zn,Pd)_xGe_{46-x}$. *J. Solid State Chem.* **2010**, *183*, 2329–2342. [CrossRef]
11. Martin, J.; Erickson, S.; Nolas, G.S.; Alboni, P.; Tritt, T.M.; Yang, J. Structural and transport properties of $Ba_8Ga_{16}Si_xGe_{30-x}$ clathrates. *J. Appl. Phys.* **2006**, *99*, 044903. [CrossRef]
12. Suekuni, K.; Avila, M.A.; Umeo, K.; Takabatake, T. Cage-size control of guest vibration and thermal conductivity in $Sr_8Ga_{16}Si_{30-x}Ge_x$. *Phys. Rev. B* **2007**, *75*, 195210. [CrossRef]

13. Nenghabi, E.N.; Myles, C.W. First-principles calculations of the vibrational and thermal properties of the type-I clathrates $Ba_8Ga_{16}Si_xGe_{30-x}$ and $Sr_8Ga_{16}Si_xGe_{30-x}$. *Phys. Rev. B* **2008**, *78*, 195202. [CrossRef]
14. Kahn, D.; Lu, J. Structural properties and vibrational modes of Si 34 and Si 46 clathrates. *Phys. Rev. B* **1997**, *56*, 13898. [CrossRef]
15. Zhao, J.; Buldum, A.; Lu, J.; Fong, C.Y. Structural and electronic properties of germanium clathrates Ge_{46} and K_8Ge_{46}. *Phys. Rev. B* **1999**, *60*, 14177. [CrossRef]
16. Biswas, K.; Myles, C.W.; Sanati, M.; Nolas, G.S. Thermal properties of guest-free Si_{136} and Ge_{136} clathrates: A first-principles study. *J. Appl. Phys.* **2008**, *104*, 033535. [CrossRef]
17. Gryko, J.; McMillan, P.F.; Sankey, O.F. NMR studies of Na atoms in silicon clathrate compounds. *Phys. Rev. B* **1996**, *54*, 3037. [CrossRef]
18. Xue, D.; Myles, C.W.; Higgins, C. Effect of guest atom composition on the structural and vibrational properties of the type II clathrate-based materials A_xSi_{136}, A_xGe_{136} and A_xSn_{136} (A = Na, K, Rb, Cs; $0 \leq x \leq 24$). *Materials* **2016**, *9*, 691. [CrossRef]
19. Kresse, G.; Furthmuller, J. Efficient iterative schemes for *ab initio* total-energy calculations using a plane-wave basis set. *Phys. Rev. B* **1996**, *54*, 11169. [CrossRef]
20. Kohn, W.; Sham, L.J. Self-consistent equations including exchange and correlation effects. *Phys. Rev.* **1963**, *140*, A1133. [CrossRef]
21. Myles, C.W.; Dong, J.; Sankey, O.F. Rattling guest atoms in Si, Ge and Sn-based Type-II clathrate materials. *Phys. Status Solidi B* **2003**, *239*, 26–34. [CrossRef]
22. Biswas, K.; Myles, C.W. Density-functional investigation of $Na_{16}A_8Ge_{136}$ (A = Rb, Cs) clathrates. *J. Phys. Condens. Matter* **2007**, *19*, 466206. [CrossRef]
23. Nolas, G.S.; Vanderveer, D.G.; Wilkinson, A.P.; Cohn, J.L. Temperature dependent structural and transport properties of the type II clathrates $A_8Na_{16}E_{136}$ (A = Cs or Rb and E = Ge or Si). *J. Appl. Phys.* **2002**, *91*, 8970–8973. [CrossRef]
24. Birch, F. Elasticity and constitution of the Earth's interior. *J. Geophys. Res.* **1952**, *57*, 227–286. [CrossRef]
25. Monkhorst, H.J.; Pack, J.D. Special points for Brillouin-zone integrations. *Phys. Rev. B* **1976**, *13*, 5188. [CrossRef]
26. Dong, J.; Sankey, O.F.; Myles, C.W. Theoretical study of the lattice thermal conductivity in Ge framework semiconductors. *Phys. Rev. Lett.* **2001**, *86*, 2361. [CrossRef] [PubMed]
27. Dong, J.; Sankey, O.F.; Ramachandran, G.K.; McMillan, P.F. Chemical trends of the rattling phonon modes in alloyed germanium clathrates. *J. Appl. Phys.* **2000**, *87*, 7726–7734. [CrossRef]
28. Nolas, G.S.; Cohn, J.L.; Slack, G.A.; Schujman, S.B. Semiconducting Ge clathrates: Promising candidates for thermoelectric applications. *Appl. Phys. Lett.* **1998**, *73*, 178–180. [CrossRef]
29. Cohn, J.L.; Nolas, G.S.; Fessatidis, V.; Metcalf, T.H.; Slack, G.A. Glasslike heat conduction in high-mobility crystalline semiconductors. *Phys. Rev. Lett.* **1999**, *82*, 779. [CrossRef]
30. Chakoumakos, B.C.; Sales, B.C.; Mandrus, D.; Nolas, G.S. Structural disorder and thermal conductivity of the semiconducting clathrate $Sr_8Ga_{16}Ge_{30}$. *J. Alloy. Compd.* **2000**, *296*, 80–86. [CrossRef]
31. Franz, R.; Wiedemann, G. Ueber die Warme-Leitungsfahigkeit der Metalle. *Annalen der Physik* **1853**, *165*, 497–531. (In German) [CrossRef]
32. Nolas, G.S.; Kendziora, C.A. Raman scattering study of Ge and Sn compounds with type-I clathrate hydrate crystal structure. *Phys. Rev. B* **2000**, *62*, 7157. [CrossRef]
33. Tadano, T.; Gohda, Y.; Tsuneyuki, S. Impact of rattlers on thermal conductivity of a thermoelectric clathrate: A first-principle study. *Phys. Rev. Lett.* **2015**, *114*, 095501. [CrossRef] [PubMed]
34. Tadano, T.; Tsuneyuki, S. Quartic anharmonicity of rattlers and its effect on lattice thermal conductivity of clathrates from first principles. *Phys. Rev. Lett.* **2018**, *120*, 105901. [CrossRef]
35. Euchner, H.; Pailhes, S.; Glordano, V.M.; de Boissieu, M. Understanding lattice thermal conductivity in thermoelectric clathrates: A density functional theory study on binary Si-based type-I clathrates. *Phys. Rev. B* **2018**, *97*, 014304. [CrossRef]
36. Norouzzadeh, P.; Krasinski, J.S.; Tadano, T. Thermal conductivity of type-I, type-II, and type-VIII pristine silicon clathrates: A first-principles study. *Phys. Rev. B* **2017**, *96*, 245201. [CrossRef]
37. Chen, C.; Zhang, Z.; Chen, J. Revisit to impacts of rattlers on thermal conductivity of clathrates. *Front. Energy Res.* **2018**, *6*, 34. [CrossRef]

38. Wei, K.; Dong, Y.; Nolas, G.S. Precursor routes to quaternary intermetallics: Synthesis, crystal structure, and physical properties of clathrate-II $Cs_8Na_{16}Al_{24}Si_{112}$. *J. Solid State Chem.* **2016**, *237*, 81–85. [CrossRef]
39. Zheng, X.; Rodriguez, S.Y.; Ross, J.H. NMR relaxation and rattling phonons in the type-I $Ba_8Ge_{16}Sn_{30}$ clathrate. *Phys. Rev. B* **2011**, *84*, 024303. [CrossRef]